2024 European Control Conference (ECC)
June 25-28, 2024. Stockholm, Sweden

Hysteresis in motion control systems: a frequency domain approach

D.W.T. Alferink, R.H.B. Fey, N. van de Wouw, M.F. Heertjes

***Abstract*— Motion stages in high-precision equipment, such as lithography machines, are typically connected to the other parts of the machine. Hysteretic behaviour of such (dynamic) links is detrimental to the tracking performance. In this paper, a quasi-linear frequency-domain approach is presented to analyze the influence of such hysteretic dynamic links on closed-loop tracking performance. The results are demonstrated by means of an industrial relevant numerical example and prove the need for development of compensation schemes for dynamic link-induced disturbances. Moreover, it is shown that hysteresis induced by dynamic links in motion systems primarily affects performance in the low frequency range.**

***Index Terms*— Dynamic links, motion stages, hysteresis, control, describing function**

I. Introduction

Due to the ever-increasing complexity and down-sizing of micro-chips, in combination with an increasing volume demand from the market, lithography machines continuously become faster and more accurate. Since these machines heavily rely on their high-precision motion stages, even these smallest sources of disturbances acting on the stages are detrimental for positioning accuracy. One of the disturbances is caused by physical connections or interfaces between stages and the rest of the machine (*the so-called dynamic links*), needed to supply for example electrical current [1], [2], [3]. An example of a dynamic link is the cable slab as illustrated in Fig. 1 for a dual-stroke wafer stage concept. These dynamic links amongst others exhibit hysteretic behavior due to internal friction, which is detrimental for tracking performance. As model-based feedforward control is a key enabler for tracking performance of high-precision motion stages [4], [5], one should consider extending the structure of the feedforward compensation in the presence of hysteresis stemming from dynamic link-induced disturbances [2], [6], which requires proper models and parameter identification.

Hysteresis is a nonlinear phenomenon that is present in many different domains such as the magnetic, mechanical, and the electrical domain [7]. It is important to remark that the definition of hysteresis has received different interpretations. As stated in [8], "The very definition of hysteresis varies from one area to another, from paper to paper." Hysteresis is usually interpreted as *i)* a time-dependent relation between input and output that cannot be expressed by a single-valued function and *ii)* that results in a looping in the input-output diagram [9]. However, many linear systems show looping behavior while these are strictly speaking not hysteretic [10]. Therefore, most publications limit the definition of hysteresis to specific properties. The most important property mentioned in a large part of the literature is that

The authors are with the Department of Mechanical Engineering, Eindhoven University of Technology, 5600 MB Eindhoven, The Netherlands, [d.w.t.alferink, r.h.b.fey, n.v.d.wouw, m.f.heertjes]@tue.nl

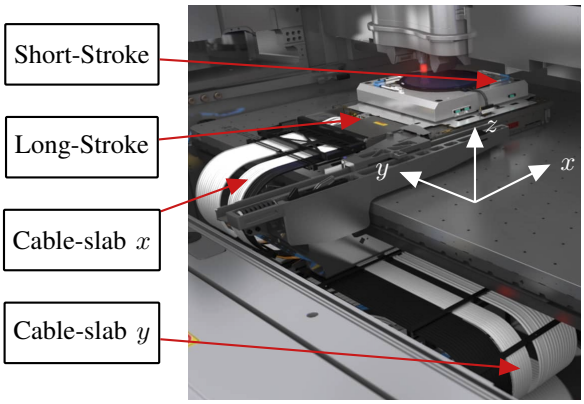

Fig. 1. Example of a dynamic link; cable slab in a wafer scanner.

hysteresis is rate-independent [10], [11], [12], [9], [13]. This means that the output only depends on the value of the input. It does not depend on its rate of change. Many different hysteresis models were developed to capture the effects of hysteresis (See e.g. [14]). Some well known examples are the Preisach model [12], Prandtl-Ishlinskii's model [7], and the Bouc-Wen model [15].

Modeling and analysis of hysteresis is widely discussed in literature as for example in piezo-electric actuators [16], [17], [18]. In this situation, the hysteresis effect is present in the input channel (externally). However, in case of motion systems, mechanical hysteresis is present as nonlinear feedback (internally) depending on the output of the system [18]. In mechanical hysteresis models, the force is chosen as the output because the mechanical hysteretic element is inducing a disturbance force onto the system based on the stage position. This makes the analysis of (internal) mechanical hysteresis different compared to external hysteresis and is much less discussed in literature [19]. In [19], a describing function approach is discussed and used to analyze open-loop dynamics, however, the detrimental effects of hysteresis in a closed-loop setting on the position error dynamics are not analyzed. In a control context, it is useful to have a closed-form expression for the describing function of the hysteresis map that gives an indication for its impact on performance in a closed-loop control setting. Therefore, the main contributions of this paper are *i)* a closed-form (frequency-domain) expression for the describing function for an elasto-plastic hysteresis model, and *ii)* providing novel and intuitive insights on how hysteresis in dynamic links affects tracking performance of a motion control application.

The remainder of the paper is organized as follows. Section II describes the problem statement in more detail. Section III presents an elasto-plastic hysteresis model and presents a quasi-linear frequency domain approach to obtain intuitive insights on closed-loop performance by using this

quasi-linear description in performance analysis. In Section IV, the feedforward mismatch due to hysteresis is discussed compared to the conventional feedforward strategy based on inverse dynamics without hysteresis. The results obtained throughout the paper are verified by an industrially relevant numerical example in Section V. Conclusions and directions for future work are given in Section VI.

II. Problem statement

A short-stroke wafer stage as illustrated in Fig. 1 is often modeled as a two-degree-of-freedom system as illustrated in Fig. 2. Here, actuation is reflected by the force $u(t)$ with $y_1(t)$ the position of actuation, and $y_2(t)$ the measured position also known as point of control (PoC). The point masses are denoted by m_1 and m_2 ($M := m_1 + m_2$) that are connected by a viscous damper with damping coefficient b and spring with stiffness k. The floating mass system is connected to the fixed world by a (nonlinear) hysteresis element $\mathscr{H}$ that represents a simplified dynamic link model for which it is valid to assume that it is much more compliant compared to the internal stiffness of the floating mass described by k. This element $\mathscr{H}$ can be described by $\phi : \mathbb{R} \to \mathbb{R}$ that maps the position $y_1(t)$ to hysteresis disturbance force $w(t)$ which gives the effective (nett) force $u(t) - w(t)$ acting on mass m_1. The transfer functions from $u - w$ to positions y_1 and y_2 are denoted by $\mathbf{P}_1(s)$ and $\mathbf{P}_2(s)$, respectively. These are given by

$$\begin{aligned} \mathbf{P}_1(s) &:= \frac{Y_1(s)}{U(s) - W(s)} = \mathbf{P}_r(s) + \mathbf{P}_{f,1}(s), \\ \mathbf{P}_2(s) &:= \frac{Y_2(s)}{U(s) - W(s)} = \mathbf{P}_r(s) - \mathbf{P}_{f,2}(s), \end{aligned} \tag{1}$$

where $\mathbf{P}_r(s) = \frac{1}{Ms^2}$ represents the rigid body dynamics and $\mathbf{P}_{f,1}(s)$ and $\mathbf{P}_{f,2}(s)$ describe the flexible dynamics of $\mathbf{P}_1(s)$ and $\mathbf{P}_2(s)$, respectively. The flexible dynamics are given by

$$\begin{aligned} \mathbf{P}_{f,1}(s) &= \frac{m_2^2}{M(m_1 m_2 s^2 + bMs + kM)}, \\ \mathbf{P}_{f,2}(s) &= \frac{m_1 m_2}{M(m_1 m_2 s^2 + bMs + kM)}, \end{aligned} \tag{2}$$

respectively. $\mathbf{P}_1(s)$ represents a collocated transfer (sensor-actuator) and $\mathbf{P}_2(s)$ represents a non-collocated transfer.

A simplified scheme for motion control systems together including this hysteresis function ϕ is illustrated in Fig. 3. Note that the system dynamics from input force $u(t)$ to PoC $y_2(t)$ is nonlinear and this system is denoted as the combined system $\hat{\mathbf{P}}$. Motion control systems heavily rely on (acceleration-)feedforward control $\mathbf{C}_{ff} = \mathbf{P}_r^{-1} \approx Ms^2$ for tracking performance (r and its derivatives are a priori known). Feedback control of such systems is primarily done

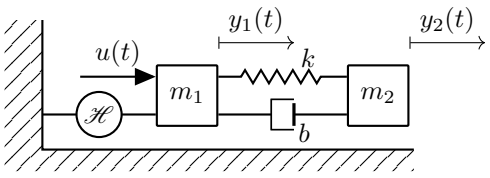

Fig. 2. Mass system with flexible dynamics including disturbance $w(t)$ induced by hysteresis element $\mathscr{H}$.

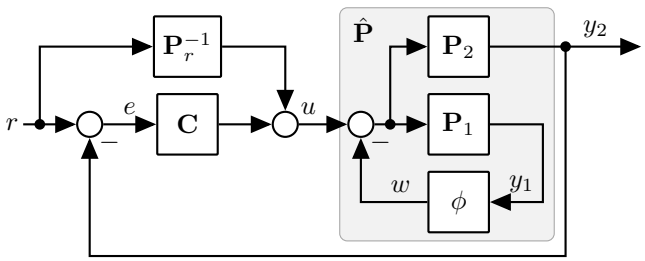

Fig. 3. Block diagram of a motion control system affected by hysteresis operator ϕ with feedback and feedforward control.

using linear controllers $\mathbf{C}$ which can be designed in the frequency-domain using loopshaping techniques. However, as the motion system combination with the hysteresis map ϕ yields a nonlinear system, it is no longer straightforward how to use such frequency-domain techniques. Therefore, this paper considers the problem of developing a quasi-linear frequency-domain model approximation for elasto-plastic (hysteresis) models ϕ. These elasto-plastic models are developed to model friction in mechanical systems [11], [14], and thus can be useful for these type of applications. When solved, this will provide frequency-domain insights into how the hysteretic behaviour of dynamics links dominantly affects positioning performance.

III. Elasto-plastic hysteresis

Elasto-plastic hysteresis models are rate-independent though input-amplitude dependent. Elasto-plastic behavior can be modeled by for example differential equation-based models such as the Jenkins model which is explained in Section III-A. Furthermore, a quasi-linear frequency-domain interpretation for this elasto-plastic model is derived in Section III-B. To conclude, the effect of hysteresis on the combined system $\hat{\mathbf{P}}$ as illustrated in Fig. 3 is discussed by means of the describing function in Section III-C.

A. Elasto-plastic (Jenkins) element

The Jenkins element contains a linear spring in series with a Coulomb friction element, see Fig. 4. The differential equation describing the dynamics of the Jenkins element is given by

$$\begin{aligned} \dot{w}(t) = &\frac{1}{2} k_J \dot{x} \{1 - \operatorname{sign}(w^2 - f_c^2) - \\ &\operatorname{sign}(\dot{x} w)(1 + \operatorname{sign}(w^2 - f_c^2))\}, \end{aligned} \tag{3}$$

where the state $w \in \mathbb{R}$ represents the force of the Jenkins element, and the input $\dot{x}$ the time-derivative of the actual displacement [1]. The model parameters are the slip-force of the Coulomb element $f_c \in \mathbb{R}_{>0}$, and the spring stiffness $k_J \in \mathbb{R}_{>0}$. In this model, the element is operating as an elastic linear spring as long as the slip-force f_c is not exceeded as shown in Fig. 5. If the force $|w| = f_c$, then the spring elongation remains constant, in other words, slipping (plastic behavior) occurs. This model's slipping behavior matches the slip of flexible wiring in the cable-slab. There are other models presented in literature to capture this phenomenon [14] but considering them falls outside of the scope of this paper.

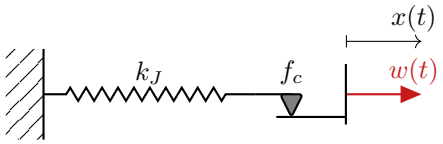

Fig. 4. Jenkins element also known as the elasto-plastic model.

B. Describing function elasto-plastic element

The describing function method [20] can be used to obtain a quasi-linear frequency-domain interpretation of the elasto-plastic models described above. With the describing function method, the contribution of the fundamental harmonic of the output signal is calculated after excitation with the input displacement $x(t) = A\sin(\omega t)$ with $A \in \mathbb{R}_{>0}$ the amplitude and $\omega \in \mathbb{R}_{>0}$ the angular excitation frequency. The higher-order harmonics are generally neglected.

For the considered elasto-plastic model, i.e., the Jenkins model, three modes of operation must be considered. Before describing each mode, we define the dimensionless coefficient

$$\zeta := \frac{f_c}{k_J A}, \tag{4}$$

for the Jenkins element. This coefficient is geometrically related to the input(x)-output(w) plot illustrated in Fig. 5. For the first mode, when $\zeta \geq 1$, the Jenkins element satisfies $k_J x \leq f_c$, $\forall t$, i.e., the Coulomb friction element does not slip. In this case, the Jenkins element will never slip and is operating in its linear range, and therefore, the transfer is simply a gain with the stiffness value k_J. For the second and third mode, the Jenkins element operates in its nonlinear range which is illustrated in Fig. 6 for sinusoidal inputs $x(t) = A\sin(\omega t)$ as the Jenkins element will slip for some t. In the second mode, the Jenkins model switches from sticking to slipping (as illustrated by the blue dots) for $xw \leq 0$, i.e., when $\zeta \in (0, 0.5]$ (note that for $\zeta = 0$, the Jenkins element gives zero output when $f_c = 0$, i.e., $\zeta = 0$). In the third mode, sticking to slipping (as illustrated by the blue dots) occurs for $xw > 0$, i.e., when $\zeta \in (0.5, 1)$ (no switching occurs for $\zeta = 1$). The distinction between these modes is important for the derivation of the describing function.

From now, we focus on the derivation of the describing function for the second mode, i.e. for $\zeta \in (0, 0.5]$. The output response of the Jenkins element after excitation by a sinusoidal displacement $x(t)$ for this mode is illustrated in Fig. 7. As shown in this figure, this output force $w(t)$ can be subdivided into five segments $i \in \{1, 2, 3, 4, 5\}$ indicated by $\textcircled{i}$ where for segment $i \in \{1, 3, 5\}$, the Coulomb element is slipping and thus $|w(t)| = f_c$. For segment $i \in \{2, 4\}$,

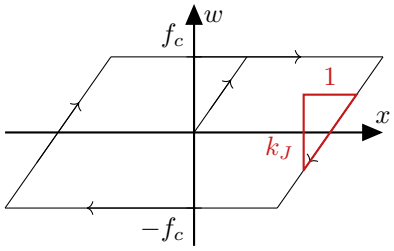

Fig. 5. Displacement-force response for sinusoidal input.

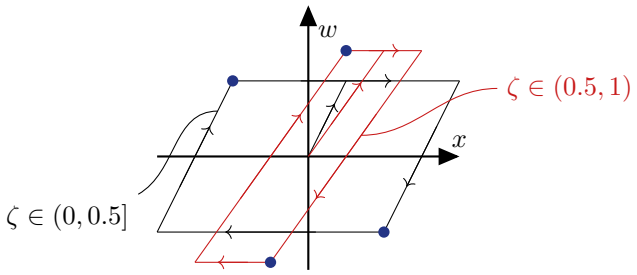

Fig. 6. Two function evaluations for the elasto-plastic Jenkins model, for $\zeta = 0.5$, switching occurs when $x = 0$ (aligned with the w-axis). The second and third mode are illustrated in black and red, respectively. Note that the increase of ζ in this particular illustration is realized by decreasing k_J and A, and increasing f_c.

the Coulomb element is sticking, hence the output force is calculated by $w(t) = k_J x(t) + w_0$ given some offset w_0 due to slipping behavior before sticking, or

$$W_i(t) = \begin{cases} f_c, & \text{if } i = 1, \\ k_J A(\sin(\omega t) - 1) + f_c, & \text{if } i = 2, \\ -f_c, & \text{if } i = 3, \\ k_J A(\sin(\omega t) + 1) - f_c, & \text{if } i = 4, \\ f_c, & \text{if } i = 5, \end{cases} \tag{5}$$

that gives the hysteretic force $w(t) = W_i(t)$ when $t \in [\tau_{i-1}, \tau_i]$ if $\zeta \in (0, 0.5]$. The switching instants are denoted by τ_i to go from sticking to slipping or vice-versa and are given on the time-axis in Fig. 7. The time instants going from sticking to slipping can be determined by the variable

$$\gamma = \arcsin(2\zeta - 1), \tag{6}$$

which can be obtained by solving $W_2(t) = W_3(t)$.

The distribution of the output force $w(t)$ in (5) is needed for the calculation of the describing function. This describing function can be calculated by

$$\mathcal{D}_\phi(b_1, a_1, A) = \frac{b_1 + a_1 j}{A}, \tag{7}$$

given the Fourier coefficients a_1, b_1 of $w(t)$ at the first frequency component. The Fourier coefficients of $w(t)$ at

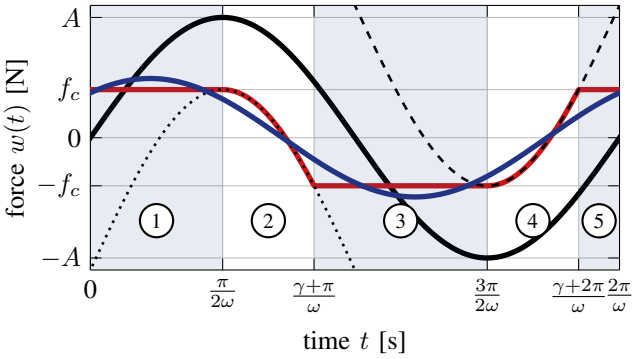

Fig. 7. Elasto-plastic hysteresis excited by input displacement $x(t)$ indicated by [——] with output force $w(t)$ indicated by [——]. The element is sticking in the region for which $W_2(t)$ and $W_4(t)$ are active (region where it coincides with [——]) illustrated by the lines [·····] and [- - -], respectively. The element is slipping in the regions highlighted by the light-blue area [▭]. First-order approximation by describing function method indicated by [——].

this fundamental harmonic can be calculated by

$$a_1 = \frac{\omega}{\pi}\sum_{i=1}^{5}\int_{\tau_{i-1}}^{\tau_i} W_i(t)\cos(\omega t)dt,$$
$$b_1 = \frac{\omega}{\pi}\sum_{i=1}^{5}\int_{\tau_{i-1}}^{\tau_i} W_i(t)\sin(\omega t)dt. \tag{8}$$

which is the sum of integrals of each function part $W_i(t) = w(t),\ \forall t \in [\tau_{i-1}, \tau_i]$. By solving (8) using (5), we obtain the Fourier coefficients

$$a_1 = \frac{4f_c}{\pi}(1-\zeta),$$
$$b_1 = \frac{4f_c}{\pi}\frac{1}{2\zeta}\left(\frac{\pi}{4} + \frac{\gamma}{2} + (2\zeta-1)\sqrt{\zeta(1-\zeta)}\right), \tag{9}$$

for the second mode $\zeta \in (0, 0.5]$. Following the same methodology for the third mode of operation $\zeta \in (0.5, 1)$, one will obtain the same expressions for a_1 and b_1 as in (9) despite the different function division $W_i(t)$. Therefore, the describing function for the full nonlinear range $\zeta \in [0, 1]$ for the Jenkins model reads

$$\mathcal{D}_\phi(k_J, \zeta) = k_J\frac{4\zeta}{\pi}\left\{\frac{1}{2\zeta}\left((2\zeta-1)\sqrt{\zeta(1-\zeta)} + \frac{\gamma}{2} + \frac{\pi}{4}\right) + (1-\zeta)j\right\}, \tag{10}$$

where $\gamma = \arcsin(2\zeta - 1)$. Note that the describing function $\mathcal{D}_\phi$ is frequency independent as expected due to the rate-independent property of the elasto-plastic model.

In the limit case $\zeta \to 0$, the describing function tends to

$$\lim_{\zeta\to 0}\mathcal{D}_\phi(k_J, \zeta) = \frac{4}{\pi}k_J\zeta j, \tag{11}$$

which is purely imaginary and, consequently, the phase is going to $\angle\mathcal{D}_\phi = 90°$ with very small magnitude. When $\zeta \to 1$, the elasto-plastic element behaves close to a linear spring and the phase goes to 0 degrees with magnitude k_J. Substitution of $\zeta = 1$ in (10) results in the linear mode of the Jenkins element, and the describing function yields $\mathcal{D}_\phi = k_J$. By plotting the magnitude and phase of $\mathcal{D}_\phi(k_J, \zeta)$ as a function of ζ as illustrated in Fig. 8 verifies these observations. Note that the magnitude of the describing function is always smaller than the spring stiffness k_J, i.e., $|\mathcal{D}_\phi| \le k_J,\ \forall\zeta \in \mathbb{R}_{\ge 0}$ in both the nonlinear and linear range of ζ.

C. Quasi-linear response of the combined system

The describing function for the Jenkins element such as derived in the previous subsection will be used for analyzing the dynamics of the combined system $\hat{\mathbf{P}}$ in the frequency domain. Using the expression $\mathcal{D}_\phi$, a quasi-linear frequency response $\hat{\mathbf{P}}^\phi(j\omega)$ can be calculated of the combined system $\hat{\mathbf{P}}$, or

$$\hat{\mathbf{P}}^\phi(j\omega) = \frac{\mathbf{P}_2(j\omega)}{1 + \mathcal{D}_\phi\mathbf{P}_1(j\omega)}, \tag{12}$$

that describes the transfer from u to output position y_2. This quasi-linear frequency response function $\hat{\mathbf{P}}^\phi(j\omega)$ is depicted in Fig. 9 for increasing values of $\zeta \in (0, 1]$ (decreasing amplitudes A) for system parameters $k_J = 10^4$ N/m, $f_c =$ 100 N, $m_1 = 5$ kg, $m_2 = 17.5$ kg, $b = 90$ Ns/m, and $k = 7.4\cdot10^7$ N/m. This figure shows that hysteresis primarily affects the low frequency range dynamics.

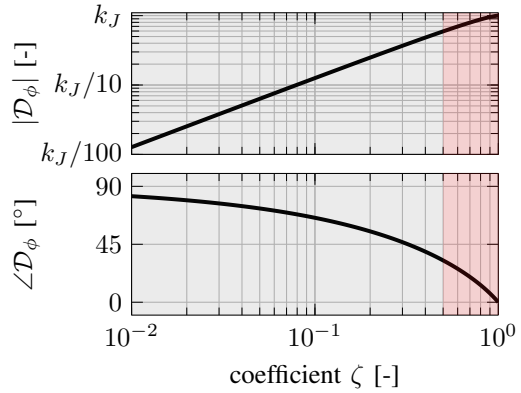

Fig. 8. Describing function $\mathcal{D}_\phi$ as a function of the dimensionless variable ζ. $\mathcal{D}_\phi$ is a small imaginary number when $\zeta \to 0$, and goes to a strictly real gain k_J when $\zeta \to 1$. For $\zeta \ge 1$, the elasto-plastic element behaves as a linear gain/spring. The gray and red area indicate the first and second mode of operation, respectively.

Remark 1: The quasi-linear frequency response of u to y_2 denoted as the combined system $\hat{\mathbf{P}}^\phi = \mathbf{P}_2(1 + \mathcal{D}_\phi\mathbf{P}_1)^{-1}$ (see Fig. 3) tends to the floating mass $\mathbf{P}_2$ for all $\zeta \in \mathbb{R}_{\ge 0}$ after the frequency

$$f^\star = \frac{1}{2\pi}\sqrt{\frac{k_J}{M}}. \tag{13}$$

The rationale behind (13) *is as follows. The magnitude of the quasi-linear $\hat{\mathbf{P}}^\phi(j\omega)$ is given by*

$$|\hat{\mathbf{P}}^\phi(j\omega)| = \left|\frac{\mathbf{P}_2(j\omega)}{1 + \mathcal{D}_\phi\mathbf{P}_1(j\omega)}\right| \ge \frac{|\mathbf{P}_2(j\omega)|}{1 + k_J|\mathbf{P}_1(j\omega)|}. \tag{14}$$

As dynamic links are much more compliant than motion stages as stated in Section II, and based on results from the describing function of $\hat{\mathbf{P}}^\phi(j\omega)$ ($k \gg k_J$) as illustrated in Fig. 9, it can be said that $\omega^\star$ satisfies $k_J|\mathbf{P}_1(j\omega^\star)| = 1$ in the rigid body region (in the region where $\mathbf{P}_r \gg \mathbf{P}_{f,i}$ for $i = 1, 2$), and therefore $\mathbf{P}_1(j\omega^\star) \approx \mathbf{P}_r(j\omega^\star)$ with $\omega^\star = 2\pi f^\star$. By substitution of $\mathbf{P}_1 = \mathbf{P}_r$, one would find (13)*. Note that this is strictly true for $\zeta \ge 1$ as for this situation, the elasto-plastic element is operating as a linear spring and the system can be reduced to the floating mass system connected to the fixed world by a linear spring with spring stiffness k_J. From this, it can be concluded that the describing function of the combined system $\hat{\mathbf{P}}^\phi(j\omega)$ tends to the floating mass transfer $\mathbf{P}_2(j\omega)$ for $\omega > \omega^\star$ for all possible operation modes of the elasto-plastic element.*

Next section will provide insights how to quantify the feedforward mismatch based on the quasi-linear frequency response $\mathcal{D}_\phi$.

IV. Feedforward mismatch due to hysteresis

In the context of Fig. 3, this section focuses on finding a relation for the feedforward mismatch on the error dynamics (e) in the presence of the hysteresis model ϕ. We will exploit the frequency-domain interpretation for ϕ via the describing function $\mathcal{D}_\phi$. For the derivation, the following type of sensitivity transfer is defined:

$$\mathbf{S}_1^\phi = (1 + \mathcal{D}_\phi\mathbf{P}_1)^{-1}, \tag{15}$$

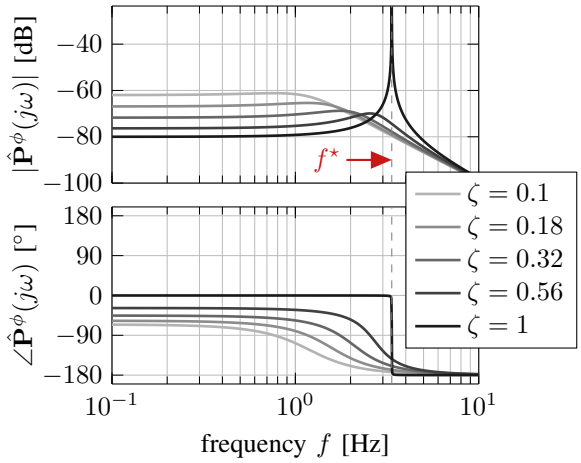

Fig. 9. Quasi-linear frequency response function $\hat{\mathbf{P}}^{\phi}(j\omega)$ for increasing $\zeta \in (0, 1]$ with 0dB = 1m/N, the resonance frequency of the two-degree-of-freedom system lies above the presented frequency range.

which indicates the transfer from $u(t)$ to $u(t) - w(t)$. The output position y_2 of the non-collocated system, i.e., the point of control is given by the describing function approximation

$$y_2 \approx \mathbf{P}_2\mathbf{P}_r^{-1}\mathbf{S}_1^{\phi}r + \mathbf{P}_2\mathbf{C}\mathbf{S}_1^{\phi}e. \tag{16}$$

This results in the quasi-linear frequency response function of the error e as a function of the reference r given by

$$e \approx \frac{1 - \mathbf{P}_2\mathbf{P}_r^{-1}\mathbf{S}_1^{\phi}}{1 + \mathbf{P}_2\mathbf{C}\mathbf{S}_1^{\phi}}r. \tag{17}$$

Eq. (17) can be used to calculate the relative difference of the error with $\mathbf{S}_1^{\phi}$ as in (15) and without ($\mathbf{S}_1^{\phi} = 1$) the dynamic link model, which gives the approximation:

$$\mathcal{E}(j\omega) := \frac{e(j\omega)}{\hat{e}(j\omega)} = \frac{(\mathbf{C}\mathbf{P}_2 + 1)(\mathbf{P}_r - \mathbf{P}_2\mathbf{S}_1^{\phi})}{\mathbf{P}_{f,2}(\mathbf{C}\mathbf{P}_2\mathbf{S}_1^{\phi} + 1)}, \tag{18}$$

where $\hat{e}(j\omega)$ describes the error with $\phi = 0$ ($\mathbf{S}_1^{\phi} = 1$). As setpoint trajectories r are dominant in the low frequency range and the dynamics of the combined system $\hat{\mathbf{P}}$ deviates from the floating mass system $\mathbf{P}_2$ in the low frequency range as shown earlier in Fig. 9, it is important to obtain intuitive insights in how the feedforward mismatch described by (18) evolves for low frequencies. This can be approximated using $\mathbf{L}(j\omega) = \mathbf{C}\mathbf{P}_2 \gg 1$, $\mathbf{P}_r(j\omega) \gg \mathbf{P}_{f,2}$ when $\omega \to 0$, and therefore it can be said that

$$\mathcal{E}(j\omega) \approx \frac{\mathbf{C}\mathbf{P}_r^2\mathcal{D}_{\phi}}{\mathbf{P}_{f,2}(\mathbf{C} + \mathcal{D}_{\phi})}, \text{ when } \omega \to 0. \tag{19}$$

In case of high-bandwidth controlled motion systems, one can make the valid assumption that $|\mathbf{C}(j\omega)| \gg |\mathcal{D}_{\phi}|$, $\forall\omega$. The approximation in (19) then further simplifies to

$$\mathcal{E}(j\omega) \approx \tilde{\mathcal{E}}(j\omega) = \mathbf{P}_r^2\mathcal{D}_{\phi}\mathbf{P}_{f,2}^{-1}, \text{ when } \omega \to 0, \tag{20}$$

where $\tilde{\mathcal{E}}$ acts as an asymptote for the error mismatch function $\mathcal{E}$ in the low-frequency range (as will be illustrated in Section V) by quadruple integrator characteristics. In the situation of the fourth-order system given in (1), the crossover frequency of this low frequency approximation ($|\tilde{\mathcal{E}}(j\omega_c)| = 1$) becomes

$$f_c = \frac{1}{2\pi}\left(\frac{k|\mathcal{D}_{\phi}|}{m_1 m_2}\right)^{\frac{1}{4}}, \ \omega_c = 2\pi f_c \tag{21}$$

which implies that for input frequencies $f_{in} < f_c$, a feedforward mismatch due to hysteresis can be expected. Note that for high frequencies, the feedforward mismatch tends to zero knowing that for $\omega \to \infty \implies \mathbf{S}_1^{\phi} \to 1$, $\mathbf{P}_r > \mathbf{P}_2$, and given the fact that the open-loop $\mathbf{L}$ generally has a positive relative degree, or $\omega \to \infty \implies \mathbf{L}(j\omega) \to 0$. This gives a high frequency approximation of (18) as

$$\hat{\mathcal{E}}(j\omega) = \mathbf{P}_r/\mathbf{P}_{f,2} = 1, \text{ when } \omega \to \infty. \tag{22}$$

In conclusion, hysteresis appears to be a low frequency range effect for motion control systems. Next section will verify the presented results by means of a numerical example.

V. Numerical Motion Control Example

The non-collocated control problem as illustrated in Fig. 2 is used to verify the results obtained in the previous sections. The control architecture as illustrated in Fig. 3 is used where the feedback controller stabilizes the closed-loop system and rejects disturbances whereas the feedforward controller is used for improved tracking. The transfer functions $\mathbf{P}_1(s)$ and $\mathbf{P}_2(s)$ as given in (1) describe the floating mass dynamics from actuator force u to position y_1 and y_2, respectively. The feedback controller $\mathbf{C}$ as in Fig. 3 is constructed by a lead-lag filter in combination with a second-order lowpass filter:

$$\mathbf{C}(s) = K\left(\frac{f_2}{f_1}\right)\frac{s + 2\pi f_1}{s + 2\pi f_2}\frac{(2\pi f_{lp})^2}{s^2 + 4\beta\pi f_{lp}s + (2\pi f_{lp})^2}. \tag{23}$$

Given the parameters as in Table I, a bandwidth frequency of $f_{bw} = 120$Hz is obtained.

TABLE I
Model, and controller parameters.

m_1	m_2	b	k	k_J	f_c	K	f_1	f_2	f_{lp}	β
5 kg	17.5 kg	90 Ns/m	$7.4 \cdot 10^7$ N/m	20 N/m	0.05 N	$6.2 \cdot 10^6$ N/m	60 Hz	240 Hz	700 Hz	0.6 [-]

The closed-loop system is excited by the reference signal $r(t) = A_r \sin(2\pi f_{in} t)$ for increasing input frequencies f_{in} with amplitude $A_r = 10$mm. The amplitude A_y of the output entering the Jenkins element (y_1) is unknown. However, in case of accurate tracking $A_r \approx A_y$. This leads to a coefficient of $\zeta = 0.25$ resulting in a magnitude of $|\mathcal{D}_{\phi}| \approx 0.3 \cdot k_J$ and phase of $\angle\mathcal{D}_{\phi} \approx 50°$ as can be seen from Fig. 8. Note that the closed-loop quasi-linear frequency response is not significantly affected as the combined plant $\hat{\mathbf{P}}$ tends to the floating mass design beyond $f^{\star} = 0.15$Hz. For small ζ this frequency is even lower due to its small gain. However, based on (21), a feedforward mismatch can be expected for input frequencies up to at least $f_c = 7.6$ Hz which is significantly higher than $f^{\star}$.

By (18), one can approximate the frequency up to which a feedforward mismatch will increase tracking errors compared to the (presumed) floating mass situation. This result is depicted in Fig. 10 and shows that there is a significant feedforward mismatch for references with sinusoids up to 10Hz.

To verify the accuracy of the describing function approach and thus our conclusions based on the feedforward mismatch obtained by quasi-linear $\mathcal{E}(j\omega)$, time-series simulations are

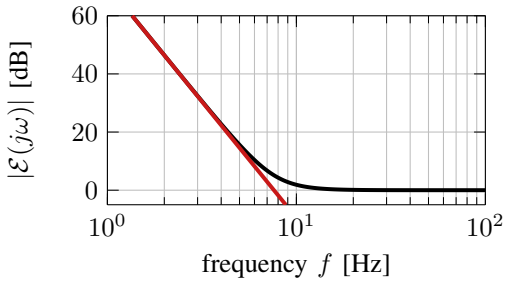

Fig. 10. Feedforward mismatch obtained by $\mathcal{E}$ in (18) indicated by [——] based on quasi-linear frequency response of hysteresis ϕ by the describing function method. The low frequency asymptotic approximation $\tilde{\mathcal{E}}(j\omega)$ as in (20) is indicated by [——].

performed. Three input frequencies $f_{in} \in \{5, 10, 15\}$Hz are used to analyze the accuracy of the describing function in a closed-loop setting and to evaluate the exact feedforward mismatch obtained from $|\mathcal{E}|$ in Fig. 10. The results are illustrated in Fig. 11 and indeed match the expected results from quasi-linear estimates $\mathcal{E}(j\omega)$. The describing function showed fairly accurate results in terms of magnitude and phase of the steady state response. The simulation results, that matches expectations from the describing function, show that the detrimental effects of hysteresis in dynamic links for input frequencies below 15 Hz from a feedforward perspective can indeed be significant. It is important to mention that stage reference trajectories have their main frequency contributions in this low frequency range. In order to improve tracking performance of reference trajectories, one should therefore extend the feedforward structure of wafer stages to deal with these detrimental hysteretic effects.

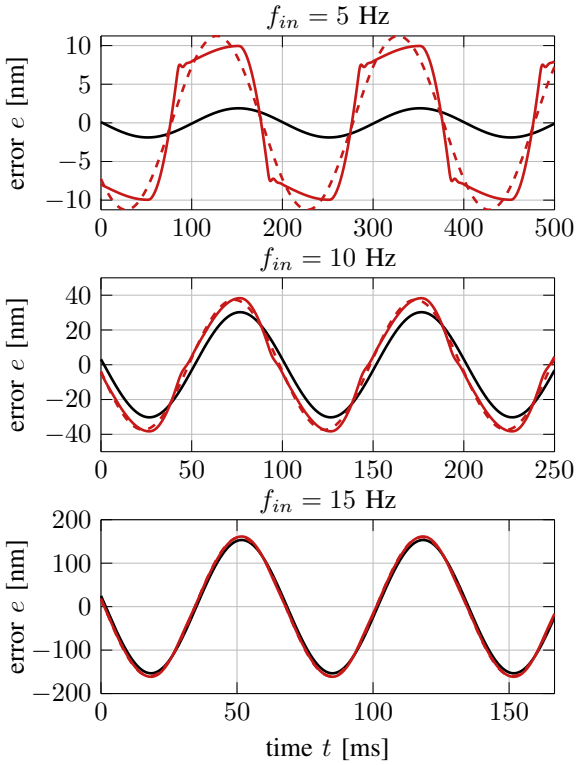

Fig. 11. Simulation results of steady-state response of the feedforward and feedback controlled two-degrees-of-freedom system with and without hysteresis, indicated by [——] and [——], respectively. The describing function approximation is indicated by [- - -].

VI. Conclusions and Future Work

This paper evaluated the effects of hysteresis in motion systems induced by a simplified model of a dynamic link system. It has been shown that the detrimental effects are dominantly present in the low frequency range. As such, it may have impact on tracking performance of scanning stages of wafer scanners. The describing function approach provides a fairly accurate approximation in terms of steady-state error magnitude and phase. However, higher-order harmonics are clearly visible and cannot be neglected for performance analysis. Future work includes modeling and identification of hysteresis models in motion control applications for feedforward purposes.

References

[1] A. Vogels, R. Fey, and M. Heertjes, "Experimental modeling of hysteresis in stage systems: A Maxwell–Iwan approach," *Mechatronics*, vol. 75, no. 102525, 2021.

[2] M. Hoogerkamp, R. Waiboer, J. van Dijk, and R. Aarts, "Attenuation of disturbances introduced by dynamic links in precision motion systems using model-based observers," *Mechatronics*, vol. 24, no. 6, 2014.

[3] M. Heertjes, H. Butler, N. Dirkx, S. van der Meulen, R. Ahlawat, K. O'Brien, J. Simonelli, K.-T. Teng, and Y. Zhao, "Control of wafer scanners: Methods and developments," in *American Control Conference*, 2020.

[4] H. Butler, "Feedforward signal prediction for accurate motion systems using digital filters," *Mechatronics*, vol. 22, 2012.

[5] P. Lambrechts, M. Boerlage, and M. Steinbuch, "Trajectory planning and feedforward design for high performance motion systems," in *American Control Conference*, 2004.

[6] R. G. Subramanian, M. Heertjes, and T. de Hoog, "A model-based inferential feedforward approach to deal with hysteresis in a motion system," in *American Control Conference*, 2018.

[7] M. Al Janaideh, M. Al Saaideh, and X. Tan, "The Prandtl–Ishlinskii hysteresis model: Fundamentals of the model and its inverse compensator [lecture notes]," *IEEE Control Systems Magazine*, vol. 43, no. 2, pp. 66–84, 2023.

[8] I. D. Mayergoyz, "Hysteresis models from the mathematical and control theory points of view," *Journal of Applied Physics*, vol. 57, pp. 3803–3805, 1985.

[9] M. Brokate and J. Sprekels, *Hysteresis and Phase Transitions*, ser. Applied Mathematical Sciences. Springer New York, 1996.

[10] K. A. Morris, "What is Hysteresis?" *Applied Mechanics Reviews*, vol. 64, no. 5, 2012.

[11] A. Visintin, *Differential Models of Hysteresis*, ser. Applied Mathematical Sciences. Springer Berlin Heidelberg, 2013.

[12] I. Mayergoyz, *Mathematical Models of Hysteresis*. Springer New York, 1991.

[13] J. W. Macki, P. Nistri, and P. Zecca, "Mathematical models for hysteresis," *SIAM Review*, vol. 35, no. 1, pp. 94–123, 1993.

[14] V. Hassani, T. Tjahjowidodo, and T. N. Do, "A survey on hysteresis modeling, identification and control," *Mechanical Systems and Signal Processing*, vol. 49, no. 1, pp. 209–233, 2014.

[15] Y.-K. Wen, "Method for random vibration of hysteretic systems," *Journal of the Engineering Mechanics Division*, vol. 102, no. 2, pp. 249–263, 1976.

[16] G.-Y. Gu, L.-M. Zhu, C.-Y. Su, H. Ding, and S. Fatikow, "Modeling and control of piezo-actuated nanopositioning stages: A survey," *IEEE Transactions on Automation Science and Engineering*, vol. 13, no. 1, pp. 313–332, 2016.

[17] H. Adriaens, W. De Koning, and R. Banning, "Modeling piezoelectric actuators," *IEEE/ASME Transactions on Mechatronics*, vol. 5, no. 4, pp. 331–341, 2000.

[18] B. Jayawardhana, H. Logemann, and E. P. Ryan, "Pid control of second-order systems with hysteresis," in *46th IEEE Conference on Decision and Control*, 2007.

[19] F. Al-Bender, W. Symens, J. Swevers, and H. Van Brussel, "Theoretical analysis of the dynamic behavior of hysteresis elements in mechanical systems," *International Journal of Non-Linear Mechanics*, vol. 39, no. 10, pp. 1721–1735, 2004.

[20] A. Gelb and W. E. V. Velde, "Multiple-input describing functions and nonlinear system design." McGraw Hill, New York, 1968.